Supporting Information

A copper(II)-based metal–organic framework: electrochemical sensor Cd(II) and Pb(II) and adsorption of organic dyes

Ting-Ting Guo,* Bing-Long Hua, Zhuo-Yi Guo, Meng-Qi Zhang, Jin-Rong Wang, Yan-Yan An, Xiao-Nan Li and Juan-Zhi Yan*

Department of Materials Science and Chemical Engineering, Taiyuan University, Taiyuan 030000, P.R. China

* Correspondence authors

E-mail: guott223@nenu.edu.cn (T.-T. Guo)

E-mail: yanjuanzhi@tyu.edu.cn (J.-Z. Yan)

Materials and instruments:

All chemicals were achieved commercially. Powder X-ray diffraction (PXRD) patterns were determined with a Rigaku SmartLab X-ray diffractometer with graphite monochromatized Cu Kα radiation (λ = 0.154 nm). FT-IR spectra were recorded with a Nicolet Magna 560 Fourier transform IR spectrometer. An elemental analyzer (Eurovector EA3000) was applied to acquire C and H data. Thermogravimetric analysis (TGA) curve was measured with a Perkin-Elmer TG-7 analyzer with 10°C per minute under nitrogen gas. The electrochemical experiments were performed using the CHI 660E electrochemical workstation from Shanghai Chenhua. X-ray photoelectron spectroscopy (XPS) was recorded on Thermo Scientific K-Alpha using a monochromatic Al Kα source (hν = 1486.6eV).

X-ray crystallography:

The crystallographic data for **Cu–L** was obtained using an Oxford Diffraction Gemini R CCD equipped with graphite-monochromated MoKα radiation (λ = 0.71073 Å). The structure was solved using direct methods with SHELXS-2018/3 and refined on F^2 by full-matrix least-squares refinement employing SHELXTL-2018/3 within WINGX.[1-3] Non-hydrogen atoms were refined anisotropically. Hydrogen atoms were added geometrically. Complete crystallographic data were given in Table S7, while selected bond lengths and bond angles were provided in Tables S8.

(1) G. M. Sheldrick, *SHELXS-2018, Programs for X-ray Crystal Structure Solution*; University of Göttingen: Göttingen, Germany, 2018.

(2) L. J. Farrugia, *WINGX: A Windows Program for Crystal Structure Analysis*; University of Glasgow: Glasgow, UK, 1988.

(3) G. M. Sheldrick, *SHELXTL-2018, Programs for X-ray Crystal Structure Refinement*; University of Göttingen: Göttingen, Germany, 2018.

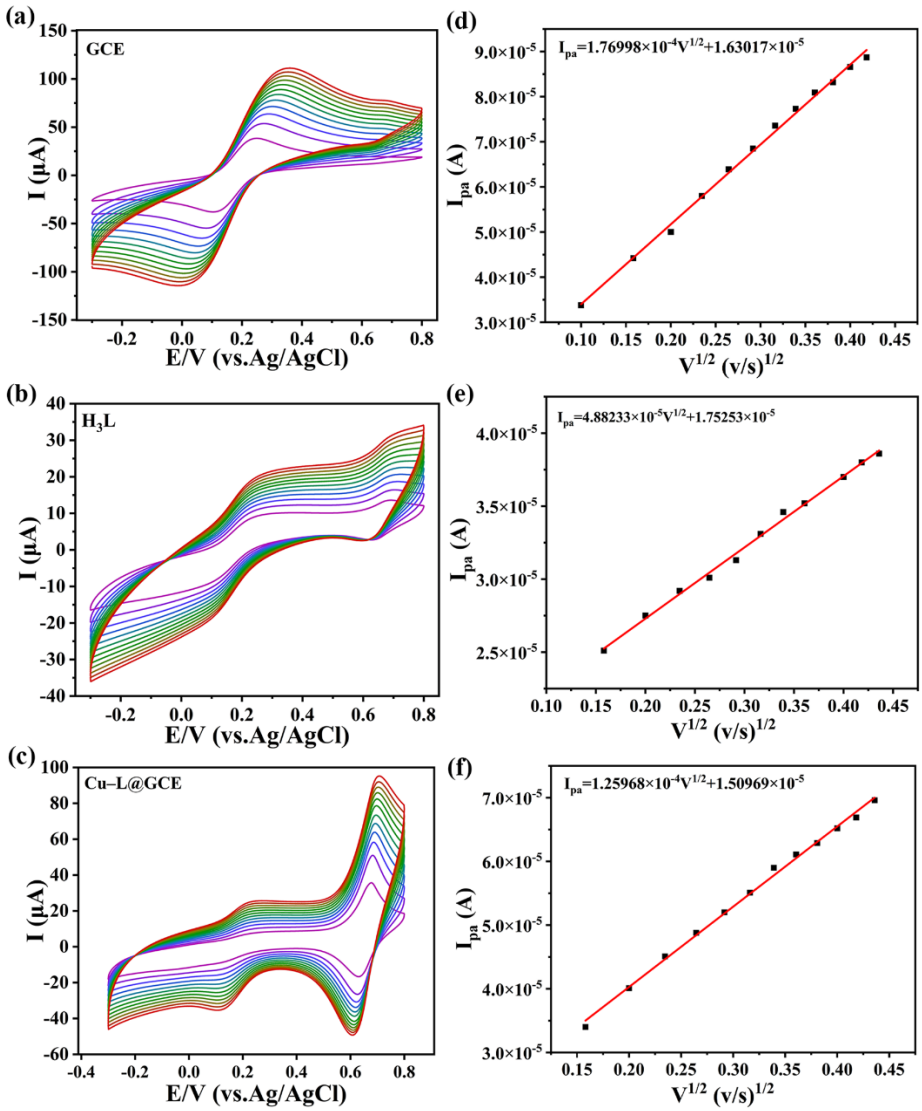

Figure S1 (a, c, e) CV records for **GCE**, **H_3L@GCE and Cu-L@GCE** in the solution of 5 mM $[Fe(CN)_6]^{3-/4-}$ and 0.1 M KCl at various scan rates (10−200 mV·s^{-1}). (b, d, f) The corresponding plot of peak currents (I_{pa}) vs the square root of scan rate.

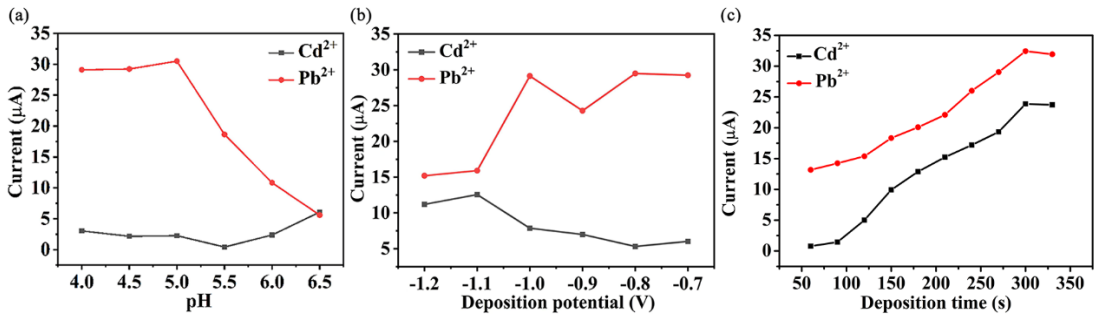

Figure S2. (a) Influence of pH values in NaAc-HAc buffer solutions for the detection of Cd^{2+} and Pb^{2+}. Optimization of deposition potentials (b), and deposition time (c) on

the stripping current responses of **Cu-L@GCE**.

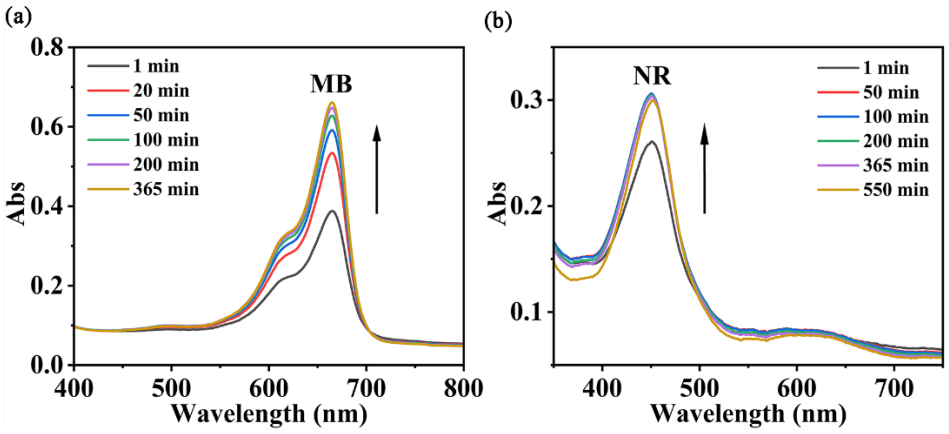

Figure S3. UV−vis absorption spectra of DMF solutions with **MB@Cu-L** (a) or **NR@Cu-L** (b) after the dye release in DMF at the given time intervals.

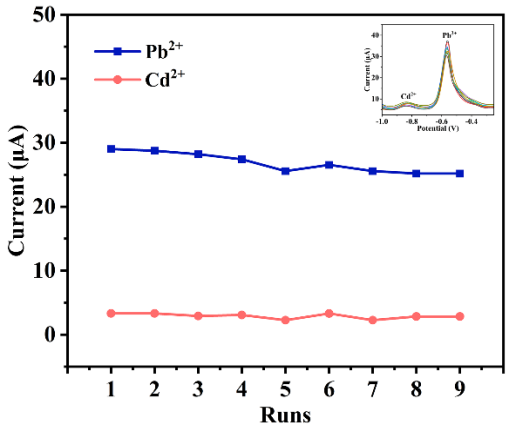

Figure S4. Reusability study of **Cu–L@GCE** in 0.1 M ABS (pH=5.0) con-taining 0.5 uM Pb(ll). Data are obtained from every SWA response shown in the inset.

Table S1 The Influence of the amount of **Cu-L@GCE** on the current of Cd^{2+} and

Pb^{2+}.

Current (μA) \ Suspension volume (μL)	3	4	5	6	7
Cd^{2+}	8.04	17.31	28.63	24.42	20.43
Pb^{2+}	9.06	22.82	32.07	28.19	26.43

Table S2 Summary electrochemical performance for determination of Cd^{2+} and Pb^{2+} with **Cu-L@GCE**.

Types	Analytes	Linear Range (μM)	Linear Regression Equation	R^2	Detection Limit (μM)
Individual determination	Cd^{2+}	8-28	I(μA)=1.2794 C(μM)-7.5025	0.9983	0.01363
	Pb^{2+}	2-14	I(μA)=3.8930 C(μM)-6.0132	0.9885	0.00212
Simultaneous determination	Cd^{2+}	10-30	I(μA)=0.6199 C(μM)-7.1965	0.9884	0.00209
	Pb^{2+}	5-15	I(μA)=6.7294C(μM)-34.4137	0.9772	0.000034

Table S3 Comparison of **Cu-L@GCE** with other materials modified electrodes for simultaneous determination of Cd^{2+} and Pb^{2+}.

Electrodes Materials	Technique	Analytes	Linear range (μM)	LOD (μM)	Ref.
UiO-66-NH_2/ GaOOH	SWASV	Cd^{2+} Pb^{2+}	0.35–1.60 0.55–2.50	0.016 0.028	(1)
Fe_2O_3/Bi_2O_3/GCE	SWASV	Cd^{2+} Pb^{2+}	0.01–1.5 0.01–2.0	0.0056 0.0036	(2)
Co-TMC4R-BDC/GCE	SWASV	Cd^{2+} Pb^{2+}	0.25-12.0 0.25-13.0	0.058 0.044	(3)

Co-TCTA	SWV	Cd^{2+} Pb^{2+}	0.4-8.0 0.4-7.0	0.071 0.022	(4)
MgFe-LDH/graphene	SWASV	Cd^{2+} Pb^{2+}	0.1–1 0.1–1	0.0059 0.0027	(5)
PProDOT(MeSH)$_2$@Si/GCE	DPV	Cd^{2+} Pb^{2+} Hg^{2+}	0.04–2.8 0.024–2.8 0.16–3.2	0.00575 0.027 0.017	(6)
Cu-L@GCE	SWV	Cd^{2+} Pb^{2+}	10–30 5–15	0.00209 0.000034	**This work**

(1) J. Ru, X. Wang, X. Cui, F. Wang, H. Ji, X. Du and X. G Lu, *Talanta,* 2021, **234**, 122679.

(2) G. Li, X. Qi, G. Zhang, S. Wang, K. Li, J. Wu, X. Wan, Y. Liu. *Microchem. J.*, 2022, **179**, 107515.

(3) F. F. Wang, C. Liu, J. Yang, H. L. Xu, W. Y. Pei, J. F. Ma, *Chem. Eng. J.*, 2022, **438**, 135639.

(4) X. T. Li, X. Niu, J. Yang, W. Y. Pei, J. F. Ma, *Microchim. Acta,* 2022, **189**, 34.

(5) Y. Ma, Y. Wang, D. Xie, Y. Gu, X. Zhu, H. Zhang, G. Wang, Y. Zhang, H. Zhao, *Chem. Eng. J.*, 2018, **347**, 953-962.

(6) M. Abdulla, A. Ali, R. Jamal, T. Bakri, W. Wu, T. Abdiryim, *Polymers*, 2019, **11**, 815.

Table S4 Comparison of **Cu-L@GCE** with other MOFs modified electrodes for simultaneous determination of Cd^{2+} and Pb^{2+}.

Electrodes	Technique	Analytes	Linear range	LOD	Ref.

Materials			(μM)	(μM)	
GA-UiO-66-NH_2/GCE	DPSV	Cd^{2+} Pb^{2+}	0.01–1.50 0.01–2.00	0.009 0.001	(1)
Co-TIC4R-I/GCE	SWASV	Cd^{2+} Pb^{2+}	0.50–7.00 0.50–7.00	0.0067 0.0027	(2)
Fe@YAU-101/GCE	DPV	Cd^{2+} Pb^{2+}	0.003–42 0.004–80	0.0001 0.00133	(3)
Cobalt zinc−zeolite imidazole framework nanofiber modified electrode	SWASV	Cd^{2+}	0.1–1000	0.02727	(4)
Co-TMC4R-BDC/GCE	SWASV	Cd^{2+} Pb^{2+}	0.25–12 0.25–13	0.058 0.044	(5)
CelloZIFPaper	LSV	Pb^{2+}	8–40	8	(6)
Cu-L@GCE	SWV	Cd^{2+} Pb^{2+}	10–30 5–15	0.00209 0.000034	**This work**

(1) M. Lu, Y. Deng, Y. Luo, J. Lv, T. Li, J. Xu, S. W. Chen and J. Wang, *Anal. Chem.*, 2019, **91**, 888−895

(2) T. T. Guo, X. Y. Cao, Y. Y. An, X. L. Zhang and J. Z. Yan, *Inorg. Chem.*, 2023, **62**, 4485−4494.

(3) Q. Liang, W. Xiao, C. Zhang, D. Zhu, S. L. Wang, S. Y. Tian, T. Long, E. L. Yue, J. J. Wang and X. Y. Hou, *Talanta*, 2023, **259**, 124491.

(4) S. Girija, S. Sam Sankar, T. Thenrajan, S. Kundu and J. Wilson, *J. Mater. Chem.*

B, 2021, **9**, 5656.

(5) F. F. Wang, C. Liu, J. Yang, H. L. Xu, W. Y. Pei and J. F. Ma, *Chem. Eng. J.*, 2022, **438**, 135639.

(6) H. N. Abdelhamid, D. Georgouvelas, U. Edlund, A. P. Mathew, *Chem. Eng. J.*, 2022, **446**, 136614.

Table S5 Water sample analysis for the detection of Cd^{2+} and Pb^{2+}**.**

Analytes	Samples	Added (μM)	Found (μM)	Recovery (%)	Relative Error (%)
Cd^{2+}	Tap water	0	–	–	–
		16	16.03	100.20	0.20
		26	26.35	101.35	1.33
	Mineral Water	0	–	–	–
		16	15.86	99.10	0.90
		26	25.61	98.51	1.51
	River water	0	–	–	–
		16	16.20	101.23	1.22
		26	25.99	99.94	0.06
Pb^{2+}	Tap water	0	–	-	-
		8	7.98	99.72	0.28
		13	12.64	97.20	2.88
	Mineral Water	0	0.39	–	–
		8	8.10	96.35	3.61
		13	13.12	97.93	2.05
	River water	0	0.24	–	–
		8	8.33	97.35	2.42
		13	13.62	97.59	2.45

The concentrations of Cd^{2+} and Pb^{2+} in environmental samples were calculated by the linear equations I (μA) = 0.6199C (μM) – 7.1965 (R^2 = 0.9884) for Cd^{2+} and I (μA) = 6.7294C (μM) – 34.4231 (R^2 = 0.9772) for Pb^{2+} of simultaneous detection. To improve accuracy, a standard addition method was employed. The values (16 and 26

μM for Cd^{2+} and 8 and 13 μM for Pb^{2+}) at both endpoints of the linear range were added.

Table S6 Comparison of **Cu-L** with other MOFs for dye adsorption.

MOFs	Organic dye	Qe / removal efficiencies	Time	Ref.
$[(CH_3)_2NH_2]_2[ZnNa_2(\mu\text{-}H_2O)_2(H_2O)_2(TATAT)]\cdot 2DMF$	MB	0.75 mg/g	24 h	(1)
Fe@Cu-MOF-2COOH Fe@Ni-MOF-2COOH	MB	38.24 mg/g 45.35 mg/g	–	(2)
$\{[Cd(PA)(4,4'\text{-bpy})_2](H_2O)\}n$	MB	29.60 mg/g	24 h	(3)
$\{[Co_4(L_1)_2(HCOO)_2(OH)_2][SiO_4(W_3O_9)_4]\}\cdot 6DMF\cdot 5H_2O$ $\{[Zn_4(L1)_2(HCOO)_2(OH)_2][SiO_4(W_3O_9)_4]\}\cdot 6DMF\cdot 5H_2O$	MB	87.2% 67.3%	48 h 48 h	(4)
$[Cd_2(Fe\text{-}L_2)_2(m_2\text{-}O)(H_2O)_2]$ $4DMF\cdot MeOH\cdot 2H_2O$ $[Cd_2(Fe\text{-}L_3)_2(m_2\text{-}O)(H_2O)_2]$ $3DMF$	MB	5.536 mg/g 3.511 mg/g	12 h 12 h	(5)
Cu-L	MB NR	12.269 mg/g 14.436 mg/g	24 h 24 h	**This work**

L_1 = a new methyl imidazole functionalized resorcin[4]arene; H_4L_2 = N,N_0-cyclohexanediaminebis-(2-hydroxyl-6-carboxy-1-naphthaldehy) and H_4L_3 = N,N_0-o-phenylenediaminebis-(2-hydroxyl-6-carboxy-1-naphthaldehy).

(1) C. Y. Sun, X. L. Wang, C. Qin, J. L. Jin, Z. M. Su, P. Huang and K. Z. Shao, *Chem.Eur. J.*, 2013, **19**, 3639-3645.

(2) M. Naqi Ahamad, M. Shahnawaz Khan, M. Shahid and M. Ahmad, *Dalton Trans.*, 2020, **49**,14690.

(3) C. Y. Sun, X. L. Wang, C. Qin, J. L. Jin, Z. M. Su, P. Huang and K. Z. Shao, *Chem. Eur. J.*, 2013, **19**, 3639-3645.

(4) Q. Y. Zhai, J. Su, T. T. Guo, J. Yang, Jian-Fang Ma, and J. S. Chen, *Cryst. Growth Des.*, 2018, **18**, 6046−6053.

(5) F. F. Wang, H. Yu, Y. Y. Liu, G. H. Xu, J. F, Ma, *Polyhedron*, 156 (2018) 188–194.

Table S7 Crystallographic Data for **Cu-L**.

Compound	**Cu-L**
Formula	$Cu_3C_{30}H_{40}N_8O_{15}S_6$
Mr	1117.70
Temperature (K)	298(2)
Crystal system	Triclinic
Space group	*P*-1
a (Å)	11.4638(10)
b (Å)	12.5600(11)
c (Å)	16.3969(14)
A (°)	77.050(3)
B (°)	78.707(3)
γ (°)	78.617(3)
V (Å^3)	2227.0(3)
Z	2
*D*calc (g·cm^{-3})	1.667
F (000)	1138
*R*int	0.0855
GOF on F^2	1.024
R_1, wR_2[I>2σ(I)]	0.0713, 0.1812
R_1, wR_2 (all data)	0.1385, 0.2191

$R_1 = \sum||F_o| - |F_c||/\sum|F_o|.wR_2 = \{\sum w[(F_o)^2 - (F_c)^2]^2/\sum w[(F_o)^2]^2\}^{1/2}$

Table S8 Selected bond distances (Å) and angles (deg) for **Cu-L.**

O(1)-Cu(2)	1.934(5)	O(4)$^{\#2}$-Cu(1)-Cu(2)	168.40(12)
O(2)-Cu(1)	1.958(5)	O(1)-Cu(2)-O(11)$^{\#3}$	171.7(2)
O(3)-Cu(2)$^{\#1}$	2.024(4)	O(1)-Cu(2)-O(7)	88.2(2)
O(4)-Cu(1)$^{\#1}$	1.978(4)	O(11)$^{\#3}$-Cu(2)-O(7)	91.7(2)
O(4)-Cu(1)$^{\#2}$	2.214(4)	O(1)-Cu(2)-O(3)$^{\#3}$	90.7(2)
O(7)-Cu(2)	2.005(4)	O(11)$^{\#3}$-Cu(2)-O(3)$^{\#3}$	87.0(2)
O(8)-Cu(1)	1.920(4)	O(7)-Cu(2)-O(3)$^{\#3}$	162.74(19)
Cu(1)-O(12)$^{\#3}$	1.966(5)	O(1)-Cu(2)-O(13)	94.1(2)
Cu(1)-Cu(2)	2.6173(11)	O(11)$^{\#3}$-Cu(2)-O(13)	94.2(2)
Cu(2)-O(11)$^{\#3}$	1.954(5)	O(7)-Cu(2)-O(13)	98.6(2)
Cu(2)-O(13)	2.149(5)	O(3)$^{\#3}$-Cu(2)-O(13)	98.7(2)
Cu(3)-O(6)$^{\#4}$	1.955(5)	O(1)-Cu(2)-Cu(1)	86.74(16)
Cu(3)-O(5)	1.956(5)	O(11)$^{\#3}$-Cu(2)-Cu(1)	85.01(15)
Cu(3)-O(9)$^{\#2}$	1.956(5)	O(7)-Cu(2)-Cu(1)	80.88(14)
Cu(3)-O(10)$^{\#5}$	1.970(5)	O(3)$^{\#3}$-Cu(2)-Cu(1)	81.86(13)
Cu(3)-O(14)	2.152(5)	O(13)-Cu(2)-Cu(1)	179.05(19)
Cu(3)-Cu(3)$^{\#4}$	2.6198(16)	O(6)$^{\#4}$-Cu(3)-O(5)	168.5(2)
C(6)-O(1)-Cu(2)	120.8(5)	O(6)$^{\#4}$-Cu(3)-O(9)$^{\#2}$	89.8(2)
C(6)-O(2)-Cu(1)	124.5(5)	O(5)-Cu(3)-O(9)$^{\#2}$	89.5(2)
C(9)-O(3)-Cu(2)$^{\#1}$	125.5(4)	O(6)$^{\#4}$-Cu(3)-O(10)$^{\#5}$	88.7(3)
C(9)-O(4)-Cu(1)$^{\#1}$	121.1(4)	O(5)-Cu(3)-O(10)$^{\#5}$	89.7(3)
C(9)-O(4)-Cu(1)$^{\#2}$	140.2(4)	O(9)$^{\#2}$-Cu(3)-O(10)$^{\#5}$	168.2(2)
Cu(1)$^{\#1}$-O(4)-Cu(1)$^{\#2}$	98.49(18)	O(6)$^{\#4}$-Cu(3)-O(14)	97.1(2)
C(13)-O(7)-Cu(2)	124.5(4)	O(5)-Cu(3)-O(14)	94.4(2)
C(13)-O(8)-Cu(1)	120.4(4)	O(9)$^{\#2}$-Cu(3)-O(14)	98.7(2)
O(8)-Cu(1)-O(2)	89.5(2)	O(10)$^{\#5}$-Cu(3)-O(14)	93.1(2)
O(8)-Cu(1)-O(12)$^{\#3}$	91.3(2)	O(6)$^{\#4}$-Cu(3)-Cu(3)$^{\#4}$	83.80(16)
O(2)-Cu(1)-O(12)$^{\#3}$	166.1(2)	O(5)-Cu(3)-Cu(3)$^{\#4}$	84.66(16)
O(8)-Cu(1)-O(4)$^{\#3}$	174.9(2)	O(9)$^{\#2}$-Cu(3)-Cu(3)$^{\#4}$	84.95(16)
O(2)-Cu(1)-O(4)$^{\#3}$	90.4(2)	O(10)$^{\#5}$-Cu(3)-Cu(3)$^{\#4}$	83.28(16)
O(12)$^{\#3}$-Cu(1)-O(4)$^{\#3}$	87.6(2)	O(14)-Cu(3)-Cu(3)$^{\#4}$	176.26(16)
O(8)-Cu(1)-O(4)$^{\#2}$	103.53(18)	C(12)-O(5)-Cu(3)	122.2(5)
O(2)-Cu(1)-O(4)$^{\#2}$	97.96(19)	C(12)-O(6)-Cu(3)$^{\#4}$	123.3(5)
O(12)$^{\#3}$-Cu(1)-O(4)$^{\#2}$	95.32(19)	C(21)-O(11)-Cu(2)$^{\#1}$	121.9(5)
O(4)$^{\#3}$-Cu(1)-O(4)$^{\#2}$	81.51(18)	C(21)-O(12)-Cu(1)$^{\#1}$	122.5(5)
O(8)-Cu(1)-Cu(2)	88.07(15)	C(24)-O(9)-Cu(3)$^{\#2}$	122.7(5)
O(2)-Cu(1)-Cu(2)	82.22(15)	C(24)-O(10)-Cu(3)$^{\#6}$	123.8(5)
O(12)$^{\#3}$-Cu(1)-Cu(2)	83.97(15)	C(28)-O(14)-Cu(3)	115.5(5)
O(4)$^{\#3}$-Cu(1)-Cu(2)	86.88(13)		

Symmetry transformations used to generate equivalent atom: $^{\#1}$x, y+1, z; $^{\#2}$-x, -y+1, -z; $^{\#3}$x, y-1, z; $^{\#4}$-x-1, -y, -z+1; $^{\#5}$x-1, y-1, z+1; $^{\#6}$x+1, y+1, z-1.